# 1.3µm Optical Interconnect on Silicon: A Monolithic III-Nitride Nanowire Photonic Integrated Circuit

Arnab Hazari<sup>1</sup>, Student Member, IEEE, Fu Chen Hsiao<sup>2</sup>, Lifan Yan<sup>3</sup>, Junseok Heo<sup>4</sup>, Member, IEEE, Joanna M. Millunchick<sup>3</sup>, John Dallesasse<sup>2</sup>, Fellow, IEEE, and Pallab Bhattacharya<sup>1</sup>, Life Fellow, IEEE

Abstract— A feasible optical interconnect on a silicon complementary metal-oxide-semiconductor (CMOS) demands epitaxial growth and monolithic integration of diode lasers and optical detectors with guided wave components on a (001) Si wafer, with all the components preferably operating in the wavelength range of 1.3 – 1.55 µm at room temperature. It is also desirable for the fabrication technique to be relatively simple and reproducible. Techniques demonstrated in the past for having optically- and electrically-pumped GaAs- and InP-based lasers on silicon include wafer bonding, selective area epitaxy, epitaxy on tilted substrates, and use of quantum dot or planar buffer layers. Here, we present a novel monolithic optical interconnect on a (001)Si substrate consisting of a III-nitride dotin-nanowire array edge emitting diode laser and guided wave photodiode, with a planar SiO<sub>2</sub>/Si<sub>3</sub>N<sub>4</sub> dielectric waveguide in between. The active devices are realized with the same nanowire heterostructure by one-step epitaxy. The electronic properties of the InN dot-like nanostructures and mode confinement and propagation in the nanowire waveguides have been modeled. The laser, emitting at the desired wavelength of 1.3 µm, with threshold current ~ 350 mA for a device of dimension 50µm×2mm, has been characterized in detail. The detector exhibits a responsivity ~0.1 A/W at 1.3 µm. Operation of the entire optical interconnect via the dielectric waveguide is demonstrated.

*Index Terms*—Indium gallium nitride, nanowires, near-infrared lasers, monolithic photodiodes, molecular beam epitaxy, silicon photonics.

This work was supported by the National Science Foundation under Grants ECCS-1648870 and DMR-1120923 (MRSEC program). J.H. was supported by "Human Resources Program in Energy Technology" of the Korea Institute of Energy Technology Evaluation and Planning (KETEP), granted financial resource from the Ministry of Trade, Industry & Energy, Republic of Korea (No. 20164030201380).

The authors are with the <sup>1</sup>Department of Electrical Engineering and Computer Science, University of Michigan, 1301 Beal Avenue, Ann Arbor, MI 48109-2122, USA, <sup>2</sup>Department of Electrical and Computer Engineering, University of Illinois at Urbana-Champaign, Urbana, Illinois 61801, USA, <sup>3</sup>Department of Material Science and Engineering, University of Michigan, Ann Arbor, MI 48109, USA, and <sup>4</sup>Department of Electrical and Computer Engineering, Ajou University, Suwon 16499, South Korea (email: harnab@umich.edu; fhsiao3@illinois.edu; ylifan@umich.edu; jsheo@ajou.ac.kr; joannamm@umich.edu; jdallesa@illinois.edu; pkb@umich.edu).

#### I. INTRODUCTION

C ince silicon with an indirect bandgap is an inefficient light-Demitting semiconductor, the common technique of incorporating an electrically-pumped laser on a silicon platform has been the integration of III - V based devices on it, either by direct epitaxy[1]–[3] or by wafer bonding[4]–[6]. Direct epitaxial growth of III-V materials and heterostructures on silicon presents three challenges. A usually large lattice mismatch leads to a high density of threading dislocations. There is also a thermal mismatch due to unequal thermal expansion coefficients. Finally, the epitaxy of polar III-V materials such as GaAs on non-polar Si leads to the formation of antiphase domains (APDs). This is usually alleviated by growing the III-V heterostructure on a (001)Si substrate offcut by 4° toward the [011] plane[1]–[3]. It is unlikely that CMOS and related Si-based technologies will be developed on such tilted platforms. Selective area epitaxy[7] and growth on special buffer layers[3], [8]–[11] have led to some success.

A very different approach to solving the Si/III-V mismatch problem is to use entirely different semiconductors, the IIInitride compounds, but not in their usual planar form. (Al, Ga, In)N nanowires and nanowire heterostructures grown catalystfree on (001)Si substrates[12]-[18] have shown extraordinary promise as crystalline (wurtzite) nanostructures for the realization of light-emitting diodes (LEDs)[19]–[22] and diode lasers[23]–[26]. Without any patterning on the substrates the nanowires grow as a random array along the c-axis and are relatively free of extended defects due to the large surface-tovolume ratio and the formation of a thin SiNx layer at the nanowire-silicon interface[21]. The SiN<sub>x</sub> layer reduces the ~13.5% stress and the defect density at the interface. Compared to planar heterostructures, the nanowires have reduced polarization field due to radial relaxation of strain during epitaxy. Consequently, the radiative recombination times are smaller than in quantum wells[18]. Thin (2-3nm) single or multiple InGaN disks can be incorporated along the length of the nanowires and the alloy composition in the disk region can be varied to yield optical emission ranging from the ultraviolet (UV) to near-infrared (near-IR)[24], [26]. It has been established that a quantum dot is formed in the disk region[27], possibly due to strain relaxation along the surface of the nanowire during epitaxy[28]. It has also been reported

that the surface recombination velocity of GaN nanowires is small and  $\sim 10^3 \text{cm/s}[29]$ . The surface state density on the nanowire walls can be further reduced by dielectric passivation[17] or by growing core-shell structures[30]. The self-organized random array of nanowires can be grown on any size of Si substrate, depending on the growth facility, and the process is therefore scalable. The nanowire area density can be varied in the range of  $10^7 - 10^{11}$  cm<sup>-2</sup> by tuning the growth parameters. Sections of the nanowires can be doped n-and p-type and thereby diodes can be easily realized.

These unique properties of III-nitride nanowires and their heterostructures provide a convenient route towards the realization of nanowire-based photonic integrated circuits with active devices on a (001)Si platform. Of particular interest is a monolithic optical interconnect consisting of a diode laser, a passive waveguide or other guided-wave elements, and a photodiode. With modulation of the laser, this would constitute an optical communication system. importantly, the desired wavelength for such a system is ~1.3 μm for eye-safe operation. Here, we demonstrate a 1.3 μm monolithic optical interconnect consisting of a InGaN/GaN dot-in-nanowire array diode laser, a SiO<sub>2</sub>/Si<sub>3</sub>N<sub>4</sub> dielectric waveguide transmission medium and a nanowire array photodiode for the first time. The interconnect has been realized by one-step epitaxy of III-nitride based nanowire heterostructure array on (001)Si, dielectric deposition, and standard device processing steps..

#### II. EPITAXY AND FABRICATION

refractive Graded index separate confinement heterostructure (GRIN-SCH) nanowire arrays, shown in Fig. 1(a), were grown by plasma-assisted molecular beam epitaxy (PAMBE) on (001)Si substrates in a Veeco GEN II system. The entire nanowire heterostructure was grown with a nitrogen plasma flow rate of 1sccm. The GaN sections were grown at a substrate temperature of 820°C, except the top p<sup>+</sup>-GaN region, which was grown at 800°C. The graded  $In_xGa_{1-x}N$  sections  $(0 \le x \le 0.4)$  forming the waveguide were grown in 10 equal steps of 15nm on both sides of the gain region consisting of 4 InN disks of thickness 6nm surrounded by 12nm In<sub>0.4</sub>Ga<sub>0.6</sub>N barriers. The graded region was grown at substrate temperatures varying from 631°C (In<sub>0.4</sub>Ga<sub>0.6</sub>N) to 819°C (GaN) and the entire InN disk/In<sub>0.4</sub>Ga<sub>0.6</sub>N barrier region was grown at 489°C. The Ga and In fluxes were in the range of  $1.1 \times 10^{-8} - 1.2 \times 10^{-7}$  Torr and  $2 \times 10^{-8} - 1 \times 10^{-7}$  Torr, respectively, depending on the composition of the material being grown. It may be noted that an electron blocking layer (EBL) has not been incorporated in the design. The electrical characteristics of the fabricated laser diodes having 15 nm Al<sub>0.15</sub>Ga<sub>0.85</sub>N EBL were substantially inferior to those without the EBL. The height, diameter and density of the nanowires are estimated to be  $\sim 700$  nm,  $\sim 60$  nm, and  $\sim 3.2 \times 10^{10}$  cm<sup>-2</sup>, and the fill factor is estimated to be 0.91. A scanning electron microscope (SEM) image of the nanowire array is shown in Fig. 1(b). Transmission electron microscopy (TEM) has been done on single InN/InGaN/GaN nanowires suitably removed from the epitaxially grown arrays and dispersed on a lacey carbon grid. High Angle Annular Dark Field (HAADF) imaging and Energy Dispersive X-ray Spectroscopy (EDX) of the active region of the nanowires (Fig. 1(c)) reveal that the InN disk regions consist of In-rich cylindrical dots with a slightly Ga-

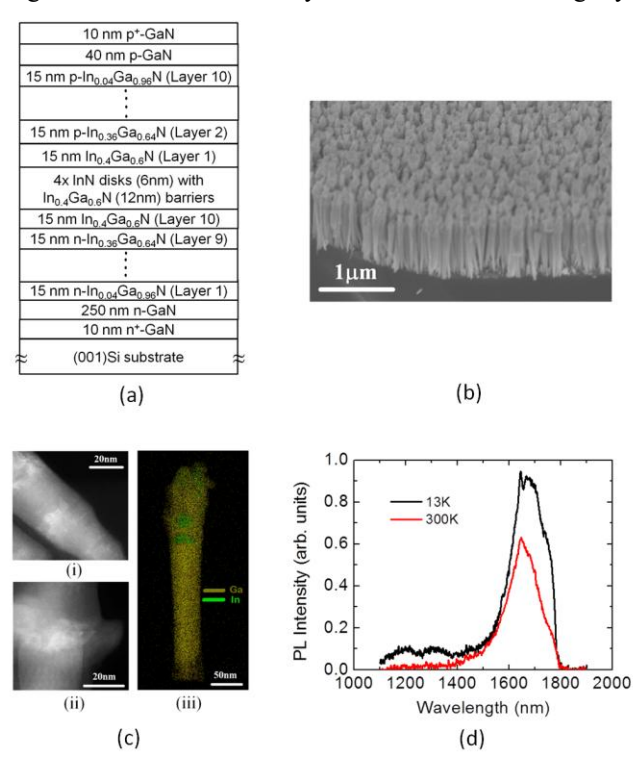


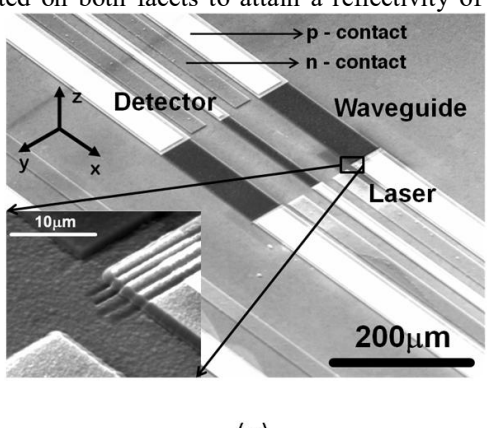
Fig. 1. InN/In<sub>0.4</sub>Ga<sub>0.6</sub>N/GaN heterostructure nanowire array laser monolithically grown on (001)Si by plasma-assisted molecular beam epitaxy. (a) Schematic of nanowire heterostructure. (b) SEM image of heterostructure nanowire array. (c) TEM-HAADF (i) and (ii) and EDS (iii) images of single nanowires showing the formation of quantum dot-like nanostructures in the InN disk regions. The bulging in the InN disk regions is clearly seen. The EDS image is from a sample with two InN disks grown directly on a section of GaN nanowire. (d) Measured room temperature and low temperature photoluminescence spectra of a nanowire array sample in which epitaxial growth was terminated after four InN/In<sub>0.4</sub>Ga<sub>0.6</sub>N disk/barrier periods. The sample was grown with optimized growth parameters described in the text. The cutoff of the PL intensity at the photon energy around 1800 nm is due the optimum response range of the detector, which is constrained by the absorption spectrum of germanium.

rich outer region. The bulging in the InN disk regions is a result of strain-driven adatom kinetics on the growing top surface of the nanowire and has been predicted by theoretical calculations[31].

Photoluminescence (PL) measurements were made at 13 K and 300 K on a sample in which growth was terminated after four periods of InN disks and  $In_{0.4}Ga_{0.6}N$  barriers and grown with the optimized parameters described earlier. The spectra recorded at 13K and 300K are illustrated in Fig. 1(d). An approximate value of the radiative efficiency ( $\eta_r$ ) of 67% is estimated from the PL peak intensities at 300K and 13K, assuming that non-radiative recombination channels are frozen at the latter temperature[32].

Fabrication of laser diodes was initiated by planarizing the nanowire array with parylene, which was deposited by physical vapor deposition (PVD) at room temperature. It has been reported that parylene is transparent at 1.3 µm[33]. Furthermore, parylene helps to passivate the nanowire surfaces and enhances the internal quantum efficiency by 10-

12%[17]. Excess parylene is etched to expose the nanowire tips, which are treated with ammonium sulfide to reduce the p-contact resistance. Ridge waveguide devices were fabricated by a combination of reactive ion etching, photolithography and contact metal deposition. The Al n-ohmic contact was formed on the Si substrate surface and the Ni/Au p-ohmic contact was formed on the top to the exposed p<sup>+</sup>-GaN nanowire tips. Ridge widths of 5 to 50 μm were defined by etching and cavity lengths of 0.5 to 2 mm were defined by dicing the substrate. This was followed by planarization with SiO<sub>2</sub> and interconnect and contact pad deposition. The cleaved facets were further polished by focused ion beam (FIB) etching using a Ga source and 3 pairs of MgF<sub>2</sub>/ZnSe (237 nm/132 nm) distributed Bragg reflectors (DBR) were deposited on both facets to attain a reflectivity of 88%. The



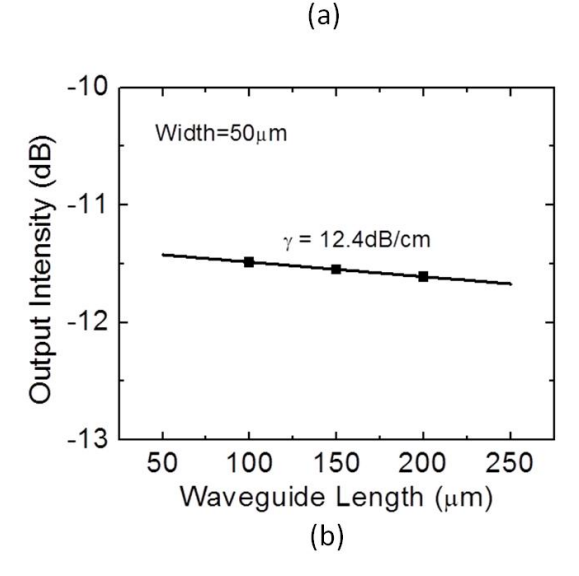


Fig. 2. Fabrication of nanowire array based photonic integrated circuit. (a) SEM image of fabricated nanowire array photonic integrated circuit consisting of nanowire diode laser, guided wave photodiode and SiO<sub>2</sub>/Si<sub>3</sub>N<sub>4</sub> dielectric waveguide in between. The inset shows a magnified image of the air/nanowire DBR mirror formed by FIB etching. (b) Measured variation of transmitted light intensity with dielectric waveguide length. The waveguides were end-fired with a constant 850 nm input excitation.

contact geometry was arranged in a ground-signal-ground configuration to facilitate high frequency probing. The laser diodes are characterized by a forward turn-on voltage of  $\sim$ 3 V, a series resistance of 10 to 25  $\Omega$ , and reverse breakdown voltage of 8 to 12 V. The fabrication of the photonic

integrated circuit follows near-identical steps (see Appendix). The dielectric waveguide in between the nanowire laser and detector is formed by selective etching of the nanowires and deposition of 400 nm  $\rm SiO_2$  followed by 400 nm of  $\rm Si_3N_4$ . For the laser, the facet away from the waveguide was made reflective by FIB etching and subsequent deposition of MgF2/ZnSe DBR layers and the facet coupled to the waveguide was made reflective with 4 pairs of air/nanowire-paralyne DBR layers, also formed by FIB etching (shown in the inset of Fig. 2(a)). For the detector, ~220 nm of anti-reflective SiO2 was deposited on the facet not coupled to the waveguide. The coupling grooves between the waveguide and the two active devices are ~5  $\mu m$ .

In addition to fabricating the entire monolithic photonic integrated circuit, we have also fabricated discrete nanowire lasers, detectors and dielectric waveguides in order to study their performance characteristics in more detail. A SEM image of the entire photonic circuit is shown in Fig. 2(a) wherein the laser, waveguide, detector and the p- and n-contacts for current injection are indicated.

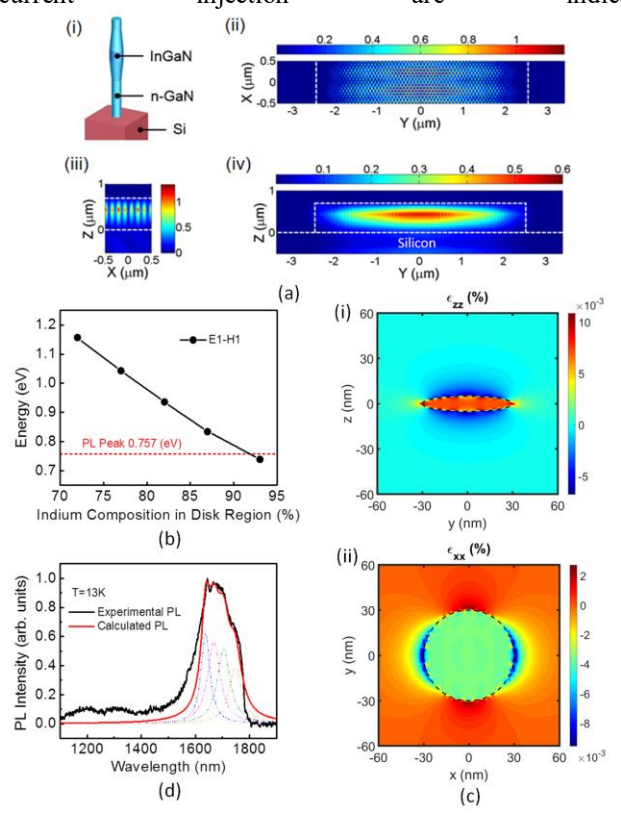


Fig. 3. Guided modes in nanowire waveguides and electronic properties of InN disks. (a) (i) Schematic diagram of the representative heterostructure nanowire considered in the 3D-FDTD simulation. (ii)-(iv) Calculated electric field intensity distribution in x-y, x-z and y-z planes. (b) Ground state transition energy (right) for a In<sub>x</sub>Ga<sub>1-x</sub>N disk (dot) with a diameter equal to 60 nm in the transverse direction and 10 nm in the longitudinal (growth) direction as a function of dot In composition x. (c) Calculated strain distribution in a In<sub>0.92</sub>Ga<sub>0.08</sub>N dot of 10nm height in the (i) out-of-plane (z), and (ii) in-plane (x-y) directions. (d) Comparison between the simulated and measured PL spectrum at 13 K for the QD structure. The dot height is 10 nm and the indium composition in the dot region equals 92% for the dominant PL peak. The dotted curves represent each component of the PL spectrum contributed by variation of the dot size and interdiffusion effects.

The propagation loss of the  $SiO_2/Si_3N_4$  dielectric waveguide was measured on control devices. Waveguides of lengths varying from 100  $\mu$ m to 200  $\mu$ m and width of 5  $\mu$ m to 50  $\mu$ m were fabricated by the deposition of 400 nm  $SiO_2$  followed by 400 nm of  $Si_3N_4$  on (001)Si substrates and subsequent photolithography and etching. The waveguides were end-fired with focused light from an 850 nm laser and the output intensity was measured with an infrared detector. The measured output as a function of guide length is plotted in Fig. 2(b), from which a propagation loss of 12.4 dB/cm is derived.

### III. PHOTON FIELD DISTRIBUTION IN NANOWIRE WAVEGUIDES

A three-dimensional (3D) finite difference time domain (FDTD) simulation was performed to characterize the field distribution and light propagation in the nanowire-parylene waveguide. The waveguide was modeled as a 700 nm thick nanowire heterostructure embedded in a 5 µm wide paryleneon-silicon ridge with a metal contact atop. The bulging InN active region in the individual nanowires due to a change of growth temperature was considered in the simulation as shown in Fig. 3(a)-(i). The diameters of GaN and InN active regions are 40 and 60 nm, respectively. The nanowire heterostructure is assumed to be identical throughout the array in the simulations for ease of calculation. The nanowires are positioned in a hexagonal close packed array with a lattice constant of 80 nm corresponding to a nanowire density of  $\sim 2.4 \times 10^{10}$  cm<sup>-2</sup>. Due to much smaller radii of the nanowires in comparison to the emission wavelength of ~1.3 μm, distributed feedback from the periodically positioned nanowires is not expected. A periodic boundary condition was applied along the light-propagating direction (x-direction) and perfectly matched layers were chosen at the other boundaries (y- and z-directions). Figures 3(a) (ii)-(iv) depict the calculated electric field distributions in the x-y, x-z, and y-z planes and the dotted white line represents the waveguide region. It was found that the waveguide supports a TE-like mode in which E<sub>v</sub> and H<sub>z</sub> are dominant and hence the light is localized between the nanowires in the y-z plane. The light is well-confined in the nanowire-parylene composite waveguide by the top electrode and the bottom silicon substrate. In particular, most of the light is confined near the bulging InN gain region because in this region the nanowires are in closer proximity, exhibiting a larger effective index. This helps in better mode confinement and reduces the optical loss to the silicon substrate.

## IV. STRAIN DISTRIBUTION AND OPTICAL TRANSITION ENERGIES IN HIGH-INDIUM QUANTUM DOTS-IN-NANOWIRES

In this section, a theoretical model for high In-content In<sub>x</sub>Ga<sub>1-x</sub>N quantum dots (QDs) is presented. The bound single-particle electron and hole states are calculated by using a fourband method. The Hamiltonian used in our model follows the derivations of Chuang[34] and Winkelnkemper[35], with the spin-orbit splitting energy assigned to zero. The band parameters are adopted from Vurgaftman[36] and Bimberg[37]. The strain distribution is taken into account by the continuum mechanical (CM) model. The TEM and the

EDX images of Fig. 1(c) reveal that the dot size fluctuates in a certain range as well as the indium composition and provide a rough estimation of dot size and indium distribution. The final geometry and indium distribution are determined by our fourband model matching the ground state transition energy to the measured PL peak. The best fit with the dominant PL peak at 1.638 µm (0.757 eV) measured at 13K occurs when the height (growth direction) of the dot is around 10 nm and the In composition inside the dot is ~92% (Fig. 3(b)). The calculated strain distribution in the dot region in the in-plane (x, y) and out-of-plane (z) directions are shown in Fig. 3(c). Figure 3(d) shows the comparison between the measured PL spectrum and the simulated values at 13 K. In this case, the height of the dot is fixed at 10nm and an indium composition in the dot region assumed to be 92% for the dominant peak (highest PL intensity). The spectrum is obtained by considering transition broadening effects with the peak wavelength calculated using the model. The multiple components with different peaks and intensities are due to slight variations in the dot size due to progressive inter-diffusion of the dot and barrier material during growth. The calculated peak intensities are at 0.7093, 0.7272, 0.7429, and 0.7569 eV, corresponding to the 4 dots in the structure. The geometry of the dot interface, which is an input parameter for our simulation model, can be modified using an error function profile to account for the interdiffusion effect. The relative intensity for each PL component is obtained by calculating the overlap between each PL component and the material gain spectrum. The observation that the shortest wavelength (highest energy) peak, which would correspond to the largest intermixing and earliest grown dot, has the highest intensity suggests that some annealing of defects may also be taking place. Under bias, the band bending caused by the strain effect is compensated by the external field. The quantum energies for electron states in the dot region are consequently raised to higher energies, while the energies for hole states are lowered. As a result, the interband transition energies should be slightly shifted toward higher values. The zero-bias electron-hole transition energies for the ground and first two excited states of the 10nm In<sub>0.92</sub>Ga<sub>0.08</sub>N quantum dot in the z-quantized direction are calculated to be 0.757, 0.823 and 0.874 eV.

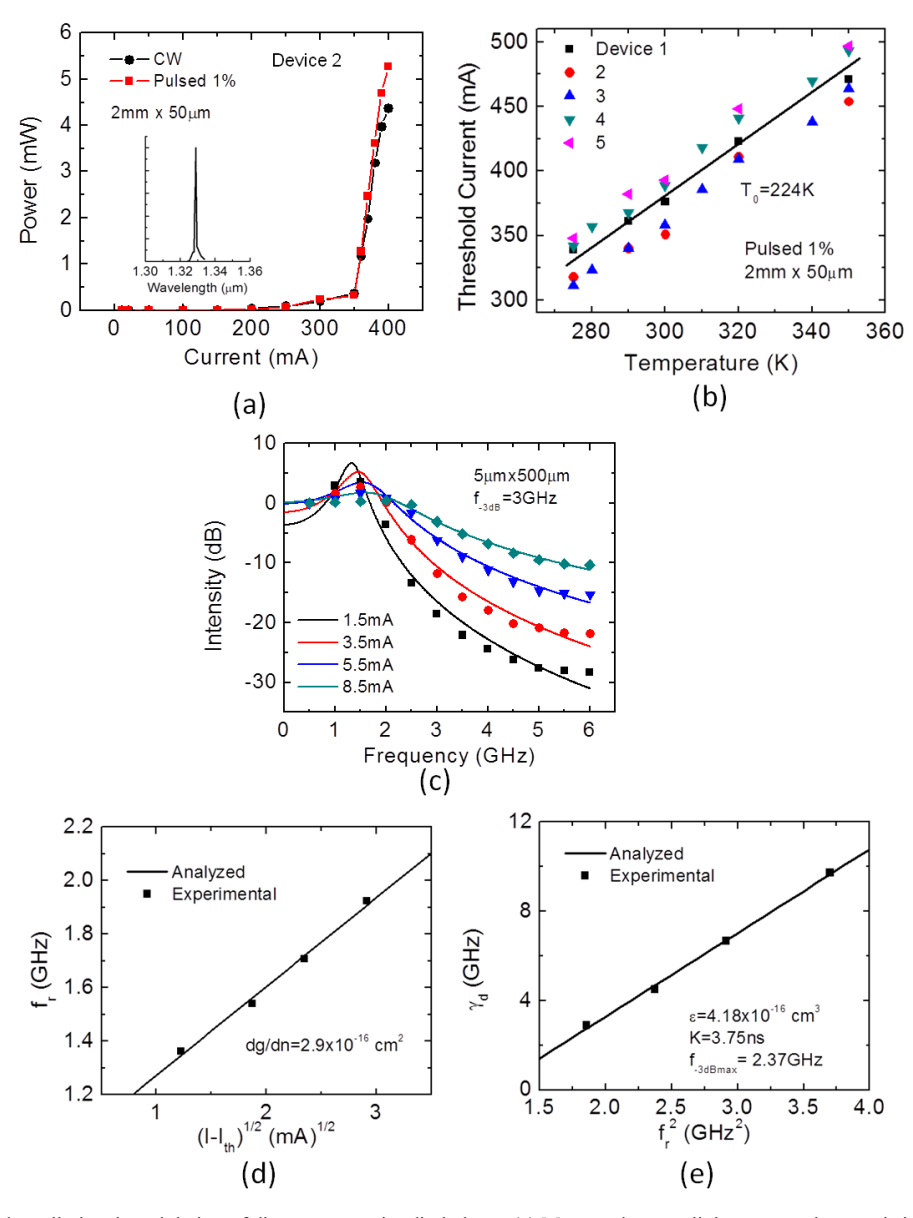


Fig. 4. Steady-state and small-signal modulation of discrete nanowire diode laser. (a) Measured output light-current characteristics of discrete edge-emitting heterostructure InN/InGaN/GaN dot-in-nanowire diode laser. The laser end mirrors are created by FIB etching followed by deposition of MgF<sub>2</sub>/ZnSe DBR. The output power is from one facet. The inset shows the spectral output for an injection  $I = 1.2I_{th}$ , where  $I_{th}$  is  $\sim 350$  mA. (b) Measured variation of threshold current with temperature of multiple devices under pulsed biasing. The solid line represents the average calculated variation. (c) Measured response of edge-emitting 1.3µm nanowire diode laser to varying high frequencies and bias currents. The values of currents shown are above the threshold current. Each point represents the peak value of the spectral output. The solid curves represent calculated modulation response in accordance with a response function incorporating damping limited operation. (d) Variation of resonance frequency derived from the data in c with square root of injection current. Analysis of the data, indicated by the solid line, yields the value of differential gain of the laser. (e) Variation of the damping factor  $\gamma_{db}$  determined from analysis of the modulation response, with square of the resonance frequency. Analysis of the data represented by the solid line is used to determine the value of the gain compression factor.

#### V. NANOWIRE ARRAY LASER AND DETECTOR

Steady state measurements were made on the discrete nanowire lasers by mounting them on a copper block without any additional heat sinking. A Peltier cooler was used to maintain the laser temperature, with active biasing, close to the ambient temperature (~300 K). Light-current (L-I) characteristics of broad area (50 µm x 2 mm) lasers were measured in both continuous wave (cw) and pulsed bias mode (20 µs pulses, 1% duty cycle), using a Keithley power source and a Newport IR detector. The L-I characteristics measured at room temperature under continuous wave (cw) and pulsed

biasing are shown in Fig. 4(a). The slope efficiency for the output with pulsed biasing is 0.12 W/A. The peak wavelength in the lasing spectrum shown in the inset is at 1.33  $\mu$ m. The blue shift of this emission from the observed spontaneous emission peak at ~1.6  $\mu$ m is believed to be due to the injection-related quantum confined Stark effect. The L-I characteristics were measured as a function of temperature by varying the temperature of the mount in the range of 275-350 K. The measured variation of the threshold current with temperature is shown in Fig. 4(b). A value of the temperature coefficient  $T_0 = 224$  K is derived from analysis of the data

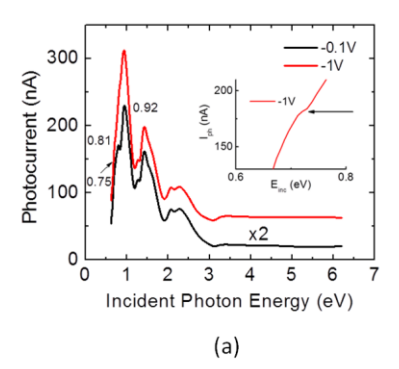
with the relation  $I_{th}$  (T) =  $I_{th}$ (0)exp(T/T<sub>0</sub>). This value to T<sub>0</sub> is much higher than those measured in 1.3 µm InGaAsP/InP quantum well lasers[38].

For an inter- and intra-chip communication link, it is necessary to transmit a modulated signal. We have therefore measured the small-signal modulation response of a discrete 5  $\mu m \times 500~\mu m$  ridge waveguide laser. The small-signal modulation response of discrete lasers were measured with a Hewlett-Packard 8350B sweep oscillator, Hewlett-Packard 83599A RF plug-in, bias T, low-noise amplifier, Newport high speed detector and Hewlett-Packard 8593A spectrum analyzer. The frequency response for varying CW injection currents (I-  $I_{\rm th}$ ) is shown in Fig. 4(c) and the data have been analyzed with the response function,

$$|R(f)|^2 \propto \frac{1}{(f^2 - f_r^2) + (\frac{\gamma_d}{2\pi})^2 f^2}$$
 (1)

where  $f_r$  is the resonance frequency and  $\gamma_d$  is the damping factor. A -3dB modulation bandwidth of 3.0 GHz is derived for an injection (I-I<sub>th</sub>) = 8.5 mA. Figure 4(d) shows a plot of  $f_r$  versus (I-I<sub>th</sub>)<sup>1/2</sup> from which a slope of 0.33 GHz/(mA)<sup>1/2</sup> is derived, which can be used to calculate the differential gain dg/dn in accordance with the relation,

$$f_r = \frac{1}{2\pi} \left[ \frac{v_g \Gamma(I - I_{th}) \frac{dg}{dn} \eta_r}{V_{act} q} \right]^{\frac{1}{2}}$$
 (2)



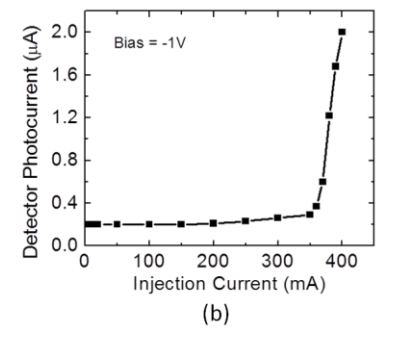


Fig. 5. Photoresponse of discrete and integrated dot-in-nanowire guided wave photodiode. (a) Photocurrent spectra of reverse biased nanowire photodiode. The devices were end-fired with light from a broadband source dispersed by a monochromator. The resonances in the spectra are attributed to interband transitions between quasi-bound states in the quantum dots formed in the InN disks. Inset shows the 0.75eV transition in the photocurrent at a bias of -1V. (b) Steady-state photocurrent of reverse biased nanowire photodiode in photonic integrated circuit in response to pulsed injection current applied to nanowire laser. The light is coupled to and guided by the dielectric waveguide to the detector.

Here  $\Gamma$  is the mode confinement factor,  $\eta_r$  is the radiative efficiency,  $v_g$  is the photon group velocity and  $V_{act}$  is the active volume of the gain medium. The value of  $\Gamma=0.0137$  is obtained from simulations based on transfer-matrix-element method assuming the laser as a planar device, which is evident from plane wave propagation based simulations described earlier. The value of  $\eta_r$  is taken to be 67%. With these values of  $\Gamma$  and  $\eta_r$ , a value of dg/dn =  $2.9\times10^{-16}$  cm² is derived. The damping factor  $\gamma_d$  derived from analysis of the modulation data is related to  $f_r$ , for damping limited operation, by the

relation 
$$\gamma_{\rm d}={\rm Kf_r^2}$$
 where  $K=4\pi^2\left(\tau_p+\frac{\epsilon}{v_g\frac{dg}{dn}}\right)$  and  $\epsilon$  is the

gain compression factor. Figure 4(e) shows the plot of  $\gamma_d$  versus  $f_r^2$ , from which we derive K=3.75 ns and  $\varepsilon=4.2x10^{-16}$  cm³, assuming a value of cavity photon lifetime  $\tau_p=3.2$  ps. The measured 3-dB bandwidth for the monolithic laser on silicon is relatively low for a variety of reasons, and can be made higher. The bandwidth, or resonance frequency  $f_r$ , is proportional to the photon density, or injection, and the differential gain. Device heating prevented measurement of the modulation response at higher injection currents. The differential gain generally decreases with bandgap energy and the value measured in this study is lower than those measured in 1.3  $\mu$ m InGaAsP/InP quantum well[39] and InAs/GaAs quantum dot lasers[40], [41].

Measurements have also been made on discrete guided wave dot-in-nanowire photodiodes to determine their performance characteristics. Spectral photocurrent measurements were made on reverse biased photodiodes (50 μm × 1mm) by end-firing them with light from a broadband source dispersed by a 0.125 nm CM110 monochromator with a spectral resolution of 0.2nm. Measurements were made at room temperature at different values of reverse bias applied to the photodiode. The resulting photocurrent was measured with a Keithley 6487 picoammeter having a resolution of 1 pA. The measured spectra are shown in Fig. 5(a). Several shoulders and peaks are observed at energies close to the absorption edge. The shoulders at  $\sim 0.75$  and 0.81 eV and a peak at approximately ~ 0.92 eV correspond to the calculated values for E<sub>1</sub>-H<sub>1</sub>, E<sub>2</sub>-H<sub>2</sub> and E<sub>3</sub>-H<sub>3</sub> transitions, respectively. Here E<sub>1,2,3</sub> are the electron ground state and first and second excited states in the conduction band. Similarly for the hole states,  $H_{1,2,3}$ . It is difficult to ascertain whether the hole states originate from heavy or light holes due to band mixing. Peaks and shoulders observed at higher energies probably originate from the graded and other regions of the nanowire heterostructure. The very slight shift in the peaks between the spectra recorded with -0.1 and -1.0 V bias is due to difference in the voltage drop across the disks. In the context of the present study, the responsivity of the photodiode at  $\sim 1.3 \mu m$  is more relevant. From the spectra recorded at -1.0 V, a responsivity of 0.11 A/W is derived, taking into account the incident power of 923 µW, a facet coupling of 0.33% and a nanowire fill factor of 0.91.

#### VI. PHOTONIC INTEGRATED CIRCUIT

Finally, we present results from measurements made on the photonic integrated circuit. We have excited the laser with a dc pulsed (20 µs pulses, 1% duty cycle) injection bias and have recorded the photocurrent response of the detector to the light emitted by the laser and coupled to the waveguide between the two devices. The laser and detector width is 50 μm, and the lengths are 2 mm and 1 mm, respectively. The SiO<sub>2</sub>/Si<sub>3</sub>N<sub>4</sub> waveguide in between is 200 μm long and 50 μm wide. The measured photocurrent of the detector biased at -1V is shown in Fig. 5(b). As expected, it follows the laser lightcurrent characteristics. A 10-fold increase in the reverse saturation current of the photodiode, from 0.2 µA to 2.0 µA is observed. Considering the measured detector responsivity of 0.11 A/W at 1.3  $\mu$ m, it is estimated that only  $\sim 20~\mu W$  of optical power is received at the input end. We believe that the factors that contribute to the loss of power emitted by the laser and ultimately coupled to the photodiode are scattering losses at the air semiconductor DBR mirror, coupling into and out of the waveguide and reflection losses at the input facet of the photodiode. We expect that the light coupled into the photodiode can be substantially increased by improved design and fabrication.

#### VII. DISCUSSION

A critical aspect of silicon photonics with CMOS circuits is that it has to be fabricated on (001)Si. The operation wavelength must also be in the eye-safe region of the spectrum. Therefore, a monolithic electrically-pumped laser, preferably emitting  $\sim 1.3$  µm light is the preferred light source. Quantum dot lasers emitting at this wavelength have been grown on silicon wafers and demonstrated. However, for reasons outlined earlier, the substrates have to be tilted from the (001) plane. On the other hand, highly mismatched GaNbased nanowires, relatively free of extended defects, can be grown on (001)Si with relative ease. A novelty of the present work rests in the fact that the gain media consists of InN disks in GaN nanowires, which have not been grown or characterized before this study. It is apparent that quantum dot-like nanostructures are formed in the disk region, accompanied by a small amount of Ga diffusion. The nonuniformity in the gain region arising principally from the nonuniformity in the InN/In<sub>0.4</sub>Ga<sub>0.6</sub>N disks which broadens the luminescence spectra and reduces the gain and differential gain of the laser. However, the non-uniformity may also broaden the spectral response of the detector.

We have successfully demonstrated the coupling of the edge emitting laser emission into a monolithic dielectric waveguide and a subsequent coupling of the guided light into an in-plane guided wave photodiode. Either passive waveguides, such as the one demonstrated here, or other guided wave components will form parts of an optical interconnect on a silicon chip. The bottom-up monolithic approach demonstrate here allows optoelectronic integration

and it is envisaged that Si-based electronic circuits for laser biasing and modulation can be incorporated. By virtue of the low growth temperature at which the nanowire heterostructures are grown it is expected that the integration will be compatible with CMOS processing of the electronics.

It is useful to note that the in-plane photodiode is realized with the same nanowire array used to fabricate the laser, thus enabling one-step epitaxy. This greatly simplifies the fabrication of the photonic integrated circuit. The detector exhibits an acceptable value of responsivity at 1.3 µm. While outside the scope of the present work, it is seen that the spectral output is characterized by sharp peaks which are believed to be due to interband transitions between discrete quasi-bound electron and hole states in the InN disks. Such features are usually observed in the absorbance spectra of quantum dots[42], providing further evidence of the formation of a quantum-dot like nanostructure in the InN disk region. It is therefore of interest to investigate intersubband transitions between conduction band states for application in infrared (IR) long wavelength detectors. The fact that such a detector could be fabricated on silicon is of great technological value.

In this study we have realized the laser and detector with a random array of dot-in-nanowire heterostructures. The nanowires are passivated with parylene and this enhances the internal quantum efficiency in all regions of the nanowire by the reduction of recombination via surface states. The efficiency could be further enhanced by growing core-shell nanowires. Also, for development purposes, an ordered array of nanowires is preferred and this can be grown on suitably patterned substrates.

#### **APPENDIX**

An appendix has been attached to this manuscript to describe the process flow of the fabrication of the photonic integrated circuit. The appendix also contains a schematic of the finished photonic integrated circuit with light trace showing the light path from the laser to the detector. Finally a plan view of the devices has also been added to further describe the structure of the devices.

#### ACKNOWLEDGMENT

This work was supported by the National Science Foundation under Grants ECCS-1648870 and DMR-1120923 (MRSEC program). J.H. was supported by "Human Resources Program in Energy Technology" of the Korea Institute of Energy Technology Evaluation and Planning (KETEP), granted financial resource from the Ministry of Trade, Industry & Energy, Republic of Korea (No. 20164030201380).

#### REFERENCES

- [1] H. Z. Chen, A. Ghaffari, H. Wang, H. Morkoc, and A. Yariv, "Low-threshold (~600 A/cm² at room temperature) GaAs/AlGaAs lasers on Si (100)," Appl. Phys. Lett., vol. 51, no. 17, pp. 1320–1321, Aug. 1987.
- [2] Z. Mi, P. Bhattacharya, J. Yang, and K. P. Pipe, "Room-temperature self-organized In<sub>0.5</sub>Ga<sub>0.5</sub>As quantum dot laser on silicon," *Electron. Lett.*, vol. 41, no. 13, pp. 742–743, Jun. 2005.

- [3] A. Y. Liu, C. Zhang, J. Norman, A. Snyder, D. Lubyshev, J. M. Fastenau, A. W. K. Liu, A. C. Gossard, and J. E. Bowers, "High performance continuous wave 1.3 μm quantum dot lasers on silicon," *Appl. Phys. Lett.*, vol. 104, no. 41104, pp. 41104-1-41104-4, Jan. 2014.
- [4] A. W. Fang, H. Park, O. Cohen, R. Jones, M. J. Paniccia, and J. E. Bowers, "Electrically pumped hybrid AlGaInAs-silicon evanescent laser," *Opt. Express*, vol. 14, no. 20, pp. 9203–9210, Sep. 2006.
- [5] D. Liang and J. E. Bowers, "Recent progress in lasers on silicon," *Nat. Photonics*, vol. 4, no. 8, pp. 511–517, Jul. 2010.
- [6] S. Tanaka, S.-H. Jeong, S. Sekiguchi, T. Kurahashi, Y. Tanaka, and K. Morito, "High-output-power, single-wavelength silicon hybrid laser using precise flip-chip bonding technology," *Opt. Express*, vol. 20, no. 27, pp. 28057–28069, Dec. 2012.
- [7] S. Lourdudoss, "Heteroepitaxy and selective area heteroepitaxy for silicon photonics," *Curr. Opin. Solid State Mater. Sci.*, vol. 16, no. 2, pp. 91–99, Mar. 2012.
- [8] M. E. Groenert, C. W. Leitz, A. J. Pitera, V. Yang, H. Lee, R. J. Ram, and E. A. Fitzgerald, "Monolithic integration of room-temperature cw GaAs/AlGaAs lasers on Si substrates via relaxed graded GeSi buffer layers," J. Appl. Phys., vol. 93, no. 1, pp. 362–367, Jan. 2003.
- [9] A. Jallipalli, M. N. Kutty, G. Balakrishnan, J. Tatebayashi, N. Nuntawong, S. H. Huang, L. R. Dawson, D. L. Huffaker, Z. Mi, and P. Bhattacharya, "1.54 μm GaSb/AlGaSb multi-quantum-well monolithic laser at 77 K grown on miscut Si substrate using interfacial misfit arrays," *Electron. Lett.*, vol. 43, no. 22, Oct. 2007.
- [10] B. Kunert, S. Zinnkann, K. Volz, and W. Stolz, "Monolithic integration of Ga(NAsP)/(BGa)P multi-quantum well structures on (0 0 1) silicon substrate by MOVPE," *J. Cryst. Growth*, vol. 310, no. 23, pp. 4776– 4779, Nov. 2008.
- [11] L. Cerutti, J. B. Rodriguez, and E. Tournie, "GaSb-based laser, monolithically grown on silicon substrate, emitting at 1.55 μm at room temperature," *IEEE Photonics Technol. Lett.*, vol. 22, no. 8, pp. 553– 555, Apr. 2010.
- [12] H.-Y. Chen, H.-W. Lin, C.-H. Shen, and S. Gwo, "Structure and photoluminescence properties of epitaxially oriented GaN nanorods grown on Si(111) by plasma-assisted molecular-beam epitaxy," *Appl. Phys. Lett.*, vol. 89, no. 243105, pp. 243105-1-243105-3, Dec. 2006.
- [13] K. Kishino, A. Kikuchi, H. Sekiguchi, and S. Ishizawa, "InGaN/GaN nanocolumn LEDs emitting from blue to red," *Proc. SPIE*, vol. 6473, p. 64730T, Feb. 2007.
- [14] R. Calarco, R. J. Meijers, R. K. Debnath, T. Stoica, E. Sutter, and H. Luth, "Nucleation and growth of GaN nanowires on Si(111) performed by molecular beam epitaxy," *Nano Lett.*, vol. 7, no. 8, pp. 2248–2251, Jun. 2007.
- [15] S. F. Li, S. Fuendling, X. Wang, S. Merzsch, M. A. M. Al-Suleiman, J. D. Wei, H.-H. Wehmann, and A. Waag, "Polarity and Its Influence on Growth Mechanism during MOVPE Growth of GaN Sub-micrometer Rods," Cryst. Growth Des., vol. 11, no. 5, pp. 1573–1577, Mar. 2011.
- [16] H. P. T. Nguyen, K. Cui, S. Zhang, S. Fathololoumi, and Z. Mi, "Full-color InGaN/GaN dot-in-a-wire light emitting diodes on silicon," Nanotechnology, vol. 22, no. 445202, pp. 1–5, Oct. 2011.
- [17] S. Jahangir, M. Mandl, M. Strassburg, and P. Bhattacharya, "Molecular beam epitaxial growth and optical properties of red-emitting (λ = 650 nm) InGaN/GaN disks-in-nanowires on silicon," *Appl. Phys. Lett.*, vol. 102, no. 71101, pp. 71101-1-71101-5, Feb. 2013.
- [18] S. Jahangir, T. Schimpke, M. Strassburg, K. A. Grossklaus, J. M. Millunchick, and P. Bhattacharya, "Red-emitting (λ = 610 nm) In<sub>0.51</sub>Ga<sub>0.49</sub>N/GaN disk-in-nanowire light emitting diodes on silicon," *IEEE J. Quantum Electron.*, vol. 50, no. 7, pp. 530–537, Jul. 2014.
- [19] A. Kikuchi, M. Tada, K. Miwa, and K. Kishino, "Growth and characterization of InGaN/GaN nanocolumn LED," *Proc. SPIE*, vol. 6129, no. 612905, pp. 612905-1-612905–8, Feb. 2006.
- [20] L. Cerutti, J. Ristic, S. Fernandez-Garrido, E. Calleja, A. Trampert, K. H. Ploog, S. Lazic, and J. M. Calleja, "Wurtzite GaN nanocolumns grown on Si(001) by molecular beam epitaxy," *Appl. Phys. Lett.*, vol. 88, no. 213114, pp. 213114-1-213114-3, May 2006.
- [21] W. Guo, M. Zhang, A. Banerjee, and P. Bhattacharya, "Catalyst-free InGaN/GaN nanowire light emitting diodes grown on (001) silicon by molecular beam epitaxy," *Nano Lett.*, vol. 10, no. 9, pp. 3355–3359, Aug. 2010.
- [22] L. Geelhaar, C. Cheze, B. Jenichen, O. Brandt, C. Pfuller, S. Munch, R. Rothemund, S. Reitzenstein, A. Forchel, T. Kehagias, P. Komninou, G. P. Dimitrakopulos, T. Karakostas, L. Lari, P. R. Chalker, M. H. Gass, and H. Riechert, "Properties of GaN nanowires grown by molecular

- beam epitaxy," IEEE J. Sel. Top. Quantum Electron., vol. 17, no. 4, pp. 878–888, Aug. 2011.
- [23] T. Frost, S. Jahangir, E. Stark, S. Deshpande, A. Hazari, C. Zhao, B. S. Ooi, and P. Bhattacharya, "Monolithic electrically injected nanowire array edge-emitting laser on (001) silicon," *Nano Lett.*, vol. 14, no. 8, pp. 4535–4541, Jul. 2014.
- [24] K. H. Li, X. Liu, Q. Wang, S. Zhao, and Z. Mi, "Ultralow-threshold electrically injected AlGaN nanowire ultraviolet lasers on Si operating at low temperature," *Nat. Nanotechnol.*, vol. 10, no. 2, pp. 140–144, Feb. 2015.
- [25] S. Jahangir, T. Frost, A. Hazari, L. Yan, E. Stark, T. LaMountain, J. Mirecki-Millunchick, B. S. Ooi, and P. Bhattacharya, "Small signal modulation characteristics of red-emitting (λ = 610 nm) III-nitride nanowire array lasers on (001) silicon," *Appl. Phys. Lett.*, vol. 106, no. 71108, Feb. 2015.
- [26] A. Hazari, A. Aiello, T.-K. Ng, B. S. Ooi, and P. Bhattacharya, "III-nitride disk-in-nanowire 1.2 μm monolithic diode laser on (001)silicon," Appl. Phys. Lett., vol. 107, no. 191107, pp. 191107-1-191107–5, Nov. 2015.
- [27] S. Deshpande, T. Frost, L. Yan, S. Jahangir, A. Hazari, X. Liu, J. Mirecki-Millunchick, Z. Mi, and P. Bhattacharya, "Formation and nature of InGaN quantum dots in GaN nanowires," *Nano Lett.*, vol. 15, no. 3, pp. 1647–1653, Feb. 2015.
- [28] H. P. T. Nguyen, S. Zhang, K. Cui, X. Han, S. Fathololoumi, M. Couillard, G. A. Botton, and Z. Mi, "p-Type modulation doped InGaN/GaN dot-in-a-wire white-light-emitting diodes monolithically grown on Si(111)," *Nano Lett.*, vol. 11, no. 5, pp. 1919–1924, Apr. 2011.
- [29] J. B. Schlager, K. A. Bertness, P. T. Blanchard, L. H. Robins, A. Roshko, and N. A. Sanford, "Steady-state and time-resolved photoluminescence from relaxed and strained GaN nanowires grown by catalyst-free molecular-beam epitaxy," *J. Appl. Phys.*, vol. 103, no. 124309, pp. 124309-1-124309–6, Jun. 2008.
- [30] H. P. T. Nguyen, M. Djavid, S. Y. Woo, X. Liu, A. T. Connie, S. Sadaf, Q. Wang, G. A. Botton, I. Shih, and Z. Mi, "Engineering the carrier dynamics of InGaN nanowire white light-emitting diodes by distributed p-AlGaN electron blocking layers," Sci. Rep., vol. 5, p. 7744, Jan. 2015.
- [31] K. Merrill, K. Yalavarthi, and S. Ahmed, "Giant growth-plane optical anisotropy in wurtzite InN/GaN disk-in-wire structures," *Superlattices Microstruct.*, vol. 52, no. 5, pp. 949–961, Apr. 2012.
- [32] Ž. Gačević, A. Das, J. Teubert, Y. Kotsar, P. K. Kandaswamy, T. Kehagias, T. Koukoula, P. Komninou, and E. Monroy, "Internal quantum efficiency of III-nitride quantum dot superlattices grown by plasma-assisted molecular-beam epitaxy," J. Appl. Phys., vol. 109, no. 10, p. 103501, May 2011.
- [33] Y. S. Jeong, B. Ratier, A. Moliton, and L. Guyard, "UV-visible and infrared characterization of poly(p-xylylene) films for waveguide applications and OLED encapsulation," *Synth. Met.*, vol. 127, no. 1, pp. 189–193, Mar. 2002.
- [34] S. L. Chuang and C. S. Chang, "k.p method for strained wurtzite semiconductors," *Phys. Rev. B*, vol. 54, no. 4, pp. 2491–2504, Jul. 1996.
- [35] M. Winkelnkemper, A. Schliwa, and D. Bimberg, "Interrelation of structural and electronic properties in In<sub>x</sub>Ga<sub>1-x</sub>N/GaN quantum dots using an eight-band k⋅p model," *Phys. Rev. B*, vol. 74, no. 155322, pp. 155322-1-155322-12, Oct. 2006.
- [36] I. Vurgaftman and J. R. Meyer, "Band parameters for nitrogencontaining semiconductors," *J. Appl. Phys.*, vol. 94, no. 6, pp. 3675– 3696, Sep. 2003.
- [37] P. Rinke, M. Winkelnkemper, A. Qteish, D. Bimberg, J. Neugebauer, and M. Scheffler, "Consistent set of band parameters for the group-III nitrides AlN, GaN, and InN," *Phys. Rev. B*, vol. 77, no. 75202, pp. 75202-1-75202–15, Feb. 2008.
- [38] P. J. A. Thijs, T. van Dongen, L. F. Tiemeijer, and J. J. M. Binsma, "High-performance λ = 1.3 μm InGaAsP-InP strained-layer quantum well lasers," *J. Light. Technol.*, vol. 12, no. 1, pp. 28–37, Jan. 1994.
- [39] H. Zhao, R. A. Arif, and N. Tansu, "Self-consistent gain analysis of type-II 'W' InGaN-GaNAs quantum well lasers," J. Appl. Phys., vol. 104, no. 43104, pp. 43104-1-43104-7, Aug. 2008.
- [40] D. Bimberg, N. Kirstaedter, N. N. Ledentsov, Z. I. Alferov, P. S. Kop'ev, and V. M. Ustinov, "InGaAs–GaAs quantum-dot lasers," *IEEE J. Sel. Top. Quantum Electron.*, vol. 3, no. 2, pp. 196–205, Dec. 1996.
- [41] P. Bhattacharya, S. Ghosh, S. Pradhan, J. Singh, Z.-K. Wu, J. Urayama, K. Kim, and T. B. Norris, "Carrier dynamics and high-speed modulation properties of tunnel injection InGaAs–GaAs quantum-dot lasers," *IEEE J. Quantum Electron.*, vol. 39, no. 8, pp. 952–962, Aug. 2003.

[42] J. Phillips, K. Kamath, and P. Bhattacharya, "Far-infrared photoconductivity in self-organized InAs quantum dots," *Appl. Phys. Lett.*, vol. 72, no. 16, pp. 2020–2022, Apr. 1998.



Arnab Hazari (Student Member, IEEE) is pursuing Ph.D. degree under the supervision of Professor Pallab Bhattacharya from the Department of Electrical Engineering and Computer Science, University of Michigan, Ann Arbor, MI, USA. He received his B.E. degree from Indian Institute of Engineering, Science and Technology, India in 2013 and M.S. degree from the Department of Electrical Engineering and Computer Science, University of Michigan in 2015. His PhD research focuses on growth and characterization of III-nitride based optoelectronic devices specifically

InN/InGaN/GaN nanowire array based lasers and detectors with operating wavelength at near-infrared on (001) Silicon.



Fu Chen Hsiao received his B.S. (2010) in physics from National Taiwan Normal University in Taiwan and M.S. (2012) in photonics engineering from National Cheng Kung University in Taiwan. He is currently working on his Ph.D. in the Department of Electrical and Computer Engineering at University of Illinois at Urbana-Champaign. His research interests include simulation of electronic, optical and transport properties of semiconductors and nanostructures, and photonic device modeling.



Lifan Yan is currently pursuing the Ph.D. degree in Material Science and Engineering from University of Michigan- Ann Arbor. She received her B.Sc. degrees in Material Science and Electrical Engineering from University of Michigan and Shanghai Jiao Tong University, respectively. Her research interests include III-V nanostructure characterization using Atom

Probe Tomography and Transmission Electron Microscopy. She has worked on multiple material systems including (In)GaN nanowire, GaSb quantum dots, GaAs nanowires.



Junseok Heo (M'12) received the B.S. degree in electrical engineering from Seoul National University, Seoul, Korea, in 2006, and the M.S. and Ph.D. degrees in electrical engineering from the University of Michigan, Ann Arbor, in 2009 and 2011, respectively. In 2012, he was a Post-Doctoral Research Fellow with the Department of Electrical Engineering and Computer Science, University of Michigan. In 2013, he joined the Department of Electrical and Computer Engineering, Ajou University as an Assistant Professor, and in 2017 became an Associate

Professor. His current research interests include III-V nanomembrane devices, III-V solar cells, nanoscale optoelectronic devices, nanophotonics, and optical ultrasound transceiver. Prof. Heo is a member of the Optical Society (OSA), the Material Research Society (MRS), SPIE, and the Optical Society of Korea (OSK).



Joanna Mirecki Millunchick is a Professor of Materials Science and Engineering, and is affiliated with the Applied Physics Program at the University of Michigan. She received her Bachelors of Science in Physics from DePaul University in Chicago in 1990, and her Ph.D. in Materials Science and Engineering from Northwestern University in Evanston in 1995. Prior to arriving at the University of Michigan in 1997, she held a postdoctoral position at Sandia National Laboratories in Albuquerque NM. Her general research interests involve manipulating

matter on the nanoscale in order to enable the design of new electronic materials for optoelectronic applications. Currently, she is working on developing nanoscale materials for solid-state lighting and energy harvesting applications. For the past several years, Millunchick has also conducted pedagogical research examining the efficacy of internet-based resources in student learning, and the impact of participation in Science and Technology related student organizations on persistence. She is the Faculty Director of M-STEM Academies in Engineering, which is a program that supports under represented students studying Science and Engineering. Prof. Millunchick has received several awards, most recently the Provost's Teaching Innovation Prize (2012) and the Raymond J. and Monica E. Schultz Outreach & Diversity Award (2015) both from the University of Michigan. In 2016 she was awarded the Arthur F. Thurnau Professorship for outstanding contributions to undergraduate education and a demonstrable impact on the intellectual development and lives of her students.



John M. Dallesasse (Fellow, IEEE) received his B.S. degree in 1985, M.S. degree in 1987, and Ph.D. degree in 1991, all from the University of Illinois at Urbana-Champaign in electrical engineering. He has over 20 years of experience in the Optoelectronics Industry, and has held a wide range of positions in technology development and management. Prior to joining the Department of Electrical and Computer Engineering at the University of Illinois in Urbana-Champaign as an Associate Professor, he was the Chief Technology Officer, Vice

President, and co-founder of Skorpios Technologies, Inc., a company involved in the integration of compound semiconductor materials with silicon in a CMOS-compatible process. John's research at the University is targeting electronic-photonic integration, novel coherent emitters for the mid-IR, and modeling of semiconductor devices. His technical contributions include, with Nick Holonyak, Jr., the discovery of III V Oxidation – an enabling technology for the fabrication of high-speed vertical-cavity surface-emitting lasers. Professor Dallesasse is a member of the American Physical Society, Tau Beta Pi, Eta Kappa Nu, and is a Fellow of the Optical Society of America and IEEE. He has over 60 publications and presentations, and 37 issued patents.



Pallab Bhattacharya (Life Fellow, IEEE) is the Charles M. Vest Distinguished University Professor of Electrical Engineering and Computer Science and the James R. Mellor Professor of Engineering in the Department of Electrical Engineering and Computer Science at the University of Michigan, Ann Arbor. He received the M. Eng. and Ph.D. degrees from the University of Sheffield, UK. He has authored the textbook Semiconductor Optoelectronic Devices (Prentice Hall, 2nd edition). His teaching and research interests are in the areas of compound semiconductors, low-

dimensional quantum confined systems, nanophotonics and optoelectronic integrated circuits. Professor Bhattacharya is a member of the US National Academy of Engineering. He has received numerous professional awards including the John Simon Guggenheim Fellowship, the Heinrich Welker Medal, the IEEE David Sarnoff Award, the Optical Society of America Nick Holonyak Award and the TMS John Bardeen Award. He is a Fellow of the IEEE, the American Physical Society, the Institute of Physics (UK), the Optical Society of America, and the National Academy of Inventors.